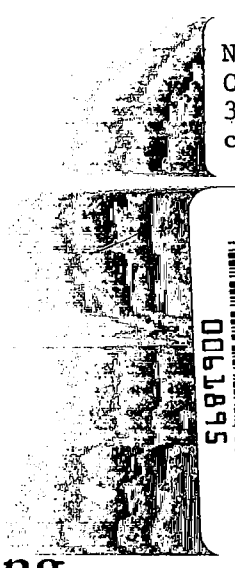



NASA Contractor Report 3046

# A Marching Method for Calculating Line and Continuum Radiation in High Energy Flow Fields



Charles W. Bolz, Jr.

CONTRACT NAS1-12527
JUNE 1979

NASA

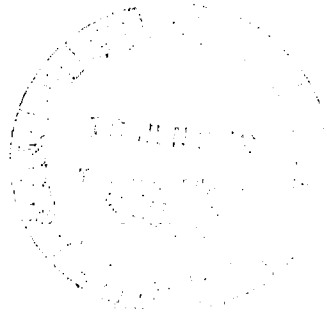

NASA Contractor Report 3046

# A Marching Method for Calculating Line and Continuum Radiation in High Energy Flow Fields

Charles W. Bolz, Jr.
*Computer Sciences Corporation*
*Hampton, Virginia*

**Prepared for**
**Langley Research Center**
**under Contract NAS1-12527**

NASA
National Aeronautics
and Space Administration

**Scientific and Technical**
**Information Office**

1979

## SUMMARY

A method is presented for calculating nongrey radiative fluxes and intensities in a highly ionized, low-temperature plasma with extreme line broadening. The method was developed to study radiative heating phenomena in the mass-injected hypersonic shock-layer environments characteristic of outer planet atmospheric entry, although it is not limited to such studies. The radiative properties model assumes local thermodynamic equilibrium and uses standard continuum and molecular band models. The atomic line model, however, uses a frequency-marching method for the frequency integration, which not only accounts completely for line overlapping (reabsorption) effects, but compares favorably in economy with the best equivalent-width methods. An assessment of hydrogen line far-wing treatments, with recommendations for engineering models, is also presented.

## LIST OF SYMBOLS

| | |
|---|---|
| $a_1$ | line frequency grid parameter defined by equation 18 |
| $a_2$ | line frequency grid parameter defined by equation 19 |
| b | line shape parameter |
| B | Planck function |
| c | constant in equation 22 |
| $c_1$ | constant in equation 23 |
| $c_2$ | constant in equation 24 |
| e | charge on an electron |
| E | black body function |
| f | line frequency grid spacing parameter |
| F | unidirectional radiative flux |
| $F_0$ | Holtsmark normal field strength |
| h | Planck's constant |
| i | index on the line frequency grid |
| I | intensity |
| J | radiosity |
| k | Boltzmann's constant |
| n | quantum number |
| n | number of frequency grid points on each side of a line center |
| N | number density |
| q | net heat flux |
| R | ratio of ion to electron impacts |
| S | ray (path) length |
| S | line strength |
| t | a dummy variable of integration (equation 8) |
| T | temperature |
| y | spatial coordinate |
| Z | radiation subgrid selection factor defined by equation 10 |

| | |
|---|---|
| $\gamma$ | line (half) half-width |
| $\varepsilon$ | emissivity |
| $\xi_3$ | exponential integral of order three |
| $\lambda$ | wavelength |
| $\mu$ | absorption coefficient |
| $\nu$ | frequency |
| $\rho$ | reflectivity |
| $\tau$ | optical depth |
| $\psi$ | line frequency grid-stretching parameter |

Subscripts

| | |
|---|---|
| c | center |
| e | electron |
| i | line frequency grid index |
| l | spatial station index |
| l | lower (absorbing) quantum level |
| L | line |
| max | maximum value |
| N | number density |
| p | plasma interaction limit |
| r | radiation |
| T | temperature |
| u | upper quantum level |
| w | quasistatic limit |
| $\nu$ | frequency |

Superscripts

| | |
|---|---|
| L | line |
| c | continuum |
| + | toward wall |
| - | toward outer boundary |
| ' | spatial derivative |

## Section 1

## INTRODUCTION

Radiation energy transport can strongly influence the wall heating and material response of an outer planet entry vehicle, both through direct heating of the vehicle wall and through coupling with the flow field. Development of useful numerical methods for predicting the radiant transport in such environments requires balancing several conflicting objectives. For example, the strongly nonlinear flow field coupling and the steep temperature and species concentration gradients within the flow field require a fine mesh and numerous solution iterations to resolve, so economical computational methods are needed. But the diversity of the radiation mechanisms involved and the spectral detail required demand that the model be comprehensive and general. Additionally, the extreme line broadening associated with highly ionized layers requires exceptional handling of the frequency integration.

Several approaches have been used for the outer planet entry radiant heating problem. Stickford and Menard (1) considered atomic and ionic atmospheric species. They used an equivalent-width model for all lines except the strong Lyman and Balmer lines of hydrogen, which were treated in full spectral detail. Poon (2) has recently extended the method to account for ablation species. Wilson (3) first computed the radiation blockage caused by ablation products for an outer planet entry, utilizing a multiband model incorporating an equivalent-width line treatment which was empirically corrected for line overlap. Wilson's radiation model was later adjusted to match results obtained by Woodward (4) who used a three-layer, spectrally detailed, uncoupled radiation model. Nicolet (5,6) reported the first practical non-hydrogenic radiation model which analytically accounted for reabsorption. This model and a derivative equivalent-width model have been used by several investigators to obtain stagnation point solutions for Jovian and Saturn entry conditions (7,8,9). A modified version of Nicolet's model was used by Moss, Anderson, and Bolz (10) to obtain the first nonsimilar downstream solutions for Jovian entry. Simplified engineering design models have been suggested by Olstad (11) and others.

All of the models discussed above are either too expensive for routine design use, or have limited accuracy or applicability. In the present report, a model is presented which accounts for all of the physical events considered in the detailed models, at a cost approaching that of the engineering design models. Full spectral line detail is assured by using a frequency-marching

integration technique which accurately accounts for atomic and ionic line broadening and reabsorption. Economy is obtained by allowing the model to discern and reject insignificant events and by using numerical techniques which minimize computer solution time.

The following sections describe the radiation transport and properties models. Uncertainties in the far-wing contribution of hydrogen lines are discussed and error bounds derived. Results are presented for benchmark cases presented in the literature to show the advantages of the frequency-marching method over the line group and equivalent-width approximations. Finally, results are presented for the stagnation point heating of a shielded probe entering the Jovian atmosphere.

## Section 2

## TRANSPORT AND PROPERTIES MODEL

### 2.1 Formulation

The transport model follows the development of Nicolet (5). The basic equation governing spectral radiation transfer in a gaseous medium in local thermodynamic equilibrium is written as

$$\frac{dI_\nu}{dS} = \bar{\mu}_\nu (B_\nu - I_\nu) \tag{1}$$

where $\bar{\mu}_\nu$ is the absorption coefficient corrected for induced emission:

$$\bar{\mu}_\nu = \mu_\nu [1 - \exp(-h\nu/kT)] \tag{2}$$

In a nonhomogeneous medium, the spectral intensity $I_\nu$ of an emitted ray varies depending on the direction of emission. For boundary and shock layer analyses, however, the directional variation is usually slight, and the tangent slab approximation may be used. This allows directional spectral fluxes to be calculated from the intensities normal to the boundary using the following expressions,

$$F_\nu^+ (y) = \int_0^{\varepsilon_b^+} E_\nu(\varepsilon_\nu^+) d\varepsilon^+ \tag{3}$$

$$F_\nu^- (y) = \int_0^{\varepsilon_b^-} E_\nu(\varepsilon_\nu^-) d\varepsilon^- + 2 J_\nu^W \xi_3 (\tau_\nu) \tag{4}$$

where the blackbody emissive power is

$$E_\nu = \pi B_\nu \tag{5}$$

the wall radiosity is

$$J_\nu^W = \varepsilon_\nu^W E_\nu(0) + \rho_\nu^W F_\nu^+(0) \tag{6}$$

the optical thickness is

$$\tau_\nu = \int_0^y \mu_\nu' \, dy \tag{7}$$

and the spectral emissivities are

$$\varepsilon_\nu^{\pm} = 1 - 2\xi_s |t_\nu - \tau_\nu| \tag{8}$$

where $t_\nu$ is a dummy value of optical depth.

To evaluate the emissivities economically, the exponential approximation

$$\varepsilon_\nu^{\pm} = 1 - \exp(-2|t_\nu - \tau_\nu|) \tag{9}$$

is often convenient. This relation is exact in the optically thick and thin limits, and results in a worst-case emissivity error of about 10% at unit optical depth.

## 2.2 Spatial Integration

Typical shock layer analyses require 50 to 100 spatial grid points to resolve all significant thermodynamic and transport events across the shock layer, while 15 to 20 points generally suffice to describe radiation transfer. The present method uses the algorithm of reference 12 to choose a radiation subgrid in equal increments of Z, where

$$Z = f \text{ (gradients of aerothermal properties across shock layer)} \tag{10}$$

The radiant transport integrals are then evaluated by representing the logarithms of the integrands as linear functions of the independent variables. Omitting the frequency subscripts for brevity, the relations

$$\mu(y) = \mu_i \left(\frac{\mu_{i+1}}{\mu_i}\right)^{\left[\frac{y - y_i}{y_{i+1} - y_i}\right]} \tag{11}$$

$$E(y) = E_i \left(\frac{E_{i+1}}{E_i}\right)^{\left[\frac{\tau - \tau_i}{\Delta\tau_i}\right]} \tag{12}$$

$$\Delta\tau_i = 2 \mu_i \Delta y \frac{\left[\frac{\mu_{i+1}}{\mu_i} - 1\right]}{\ell_n \left[\frac{\mu_{i+1}}{\mu_i}\right]} \tag{13}$$

yield the recursion formula for F

$$F_i^+ = e^{-\Delta\tau_i}\left[F_{i+1}^+ + \frac{E_i\, e^{-\Delta\tau_i} - E_{i+1}}{1 + \frac{1}{\Delta\tau_i}\ln\frac{E_i}{E_{i+1}}}\right] \tag{14}$$

A similar relation is found for $F_i^-$ by evaluating equation 14 in the opposite direction.

## 2.3 Frequency Grid

The total radiative flux at any point y is found by integrating the monochromatic fluxes given by equation 14 over the spectrum;

$$q_r(y) = \int_0^\infty [F_\nu^+(y) - F_\nu^-(y)]\, d\nu \tag{15}$$

Before choosing the frequency grid, it is convenient to separate the transport integrals into line and continuum components as follows:

$$F_\nu^L = F_\nu - F_\nu^C \tag{16}$$

This allows independent selection of the line and continuum frequency grids, and assessment of the importance of line effects.

For the continuum, the frequency grid must describe the variation in the Planck function, the continuum absorption coefficients, and the molecular band coefficients. The first requirement is met by distributing nodal points at roughly even intervals across the frequency range, $0.02\ \text{eV} \leq h\nu \leq 12kT_{max}$, where $T_{max}$ is the maximum temperature in the layer. This also satisfies the second requirement except in the ultraviolet, where frequency points must be placed to resolve the atomic photoionization thresholds. The molecular rotational and vibrational line bands, which are treated as pseudo-continuum, are adequately represented by distributing grid points at the borders of the band, and at two to five interior frequencies, depending on the importance of the species.

Evaluation of the atomic and ionic line contributions requires selection of a frequency grid for each line; this grid must characterize both the line and the layer. To reflect these requirements, a grid-stretching parameter, $\psi$, is defined, and the grid spacing established using a growth law, as follows:

$$\psi = \gamma(\bar{y}) \, (1 + \tau_c)^{1/2} \tag{17}$$

$$|\nu - \nu_c|_1 = a_1 \psi \tag{18}$$

$$|\nu - \nu_c|_{max} = a_2 \psi \tag{19}$$

$$|\nu - \nu_c|_i = a_1 \psi (1 + f)^{i-1} \tag{20}$$

The line (half) half-width $\gamma(\bar{y})$ is evaluated at that point in the layer where the product of the line strength, S, and half-width, $\gamma$, is a maximum; this avoids choosing an overly coarse grid for ablation species which are often significant in the radiation calculation only near the wall. The optical depth is for the entire layer at the frequency of the line center. The stretching parameter thus approximates the distance to the half intensity position for weak lines, and to the frequency at which the layer has unit optical depth for strong lines.* The constants $a_1$ and $a_2$ are set to 0.5 and 10, respectively; these values assure representative placement of points over the non-black wings of strong lines, while incorporating over 90% of the contribution of weak lines. The growth factor, f, is defined by the relation

$$\nu_n - \nu_c = (\nu_1 - \nu_c) \, (1 + f)^{n-1} \tag{21}$$

*where n is the number of frequency increments on each side of the line. Five to nine increments* are used on each side of the line, depending on the line's contribution to the total radiative transport.

## 2.4 Frequency-Marching Method

The generality and economy of the present calculation method is obtained by using a frequency-marching method to integrate equation 15. This method (illustrated in Figure 1) proceeds line by line through the spectrum as outlined below. For each line and spatial station:

(1) A frequency grid is established for the core of the current line using equations 17 through 21. The absorption coefficient array is initialized at the current value of the continuum coefficient. Then the line contributions due to Stark, Doppler, and resonance broadening are computed

---

*For a strong Lorentzian line, $\tau_c >> 1$, in a homogeneous layer with an insignificant continuum, the frequency separation to the point where the layer has unit optical depth is:

$$\frac{(\tau = 1)}{\tau_c} = \frac{\gamma^2}{\gamma^2 + \Delta\nu^2} \; ; \; \Delta\nu = \gamma(\tau_c - 1)^{1/2} \approx (\tau_c + 1)^{1/2}$$

at each grid point and summed into the array.

(2) Next, the Stark effect absorption contribution of each overlapping line wing is calculated at three grid points, curve fit at the remaining points, and summed into the absorption coefficient array of the current line. (The wings of resonance and Doppler broadened lines are insignificant.) A line is considered to overlap the current line if the frequency separation of the line centers is less than the effective width of the overlapping line, as given by equation 19.

(3) The total absorption coefficients thus found are corrected for induced emission, and the bi-directional fluxes for the current line computed.

(4) The procedure is repeated for the next line. If this line is centered in a new continuum interval, a new value is computed for the continuum absorption coefficient. Continuum absorption is evaluated at the midpoint of continuum intervals. Note that the line frequency grid need not be contained in the current continuum interval; in fact, the grid can straddle two (or more) continuum intervals, as shown in Figure 1.

(5) If no line is centered in the current continuum interval, a dummy line is placed at the interval midpoint, and a frequency grid established to correctly account for the wings of lines in adjacent continuum intervals.

This procedure avoids the inherent errors and inefficiencies of the line group approximation, which must treat all lines as fully overlapped with lines within a group, and isolated from lines in adjacent groups. It also provides a more realistic treatment of line overlapping than is possible using equivalent-width models, at a modest increase in computational requirements.

## 2.5 Radiation Properties Model

The radiation properties model is adapted largely from the Aerotherm RAD/69 and RAD/73 radiation codes (5,6,13,14). Continuum and line contributions to the absorption coefficient are computed independently for each species and mechanism and summed. Continuum mechanisms considered include photoionization, photodetachment, free-free dissociation, and photodissociation. Atomic line broadening mechanisms include electron impact (Stark), resonance, and Doppler; ion impact effects are considered for hydrogen at high densities. Local thermodynamic equilibrium is assumed. Plasma interactions are ignored.

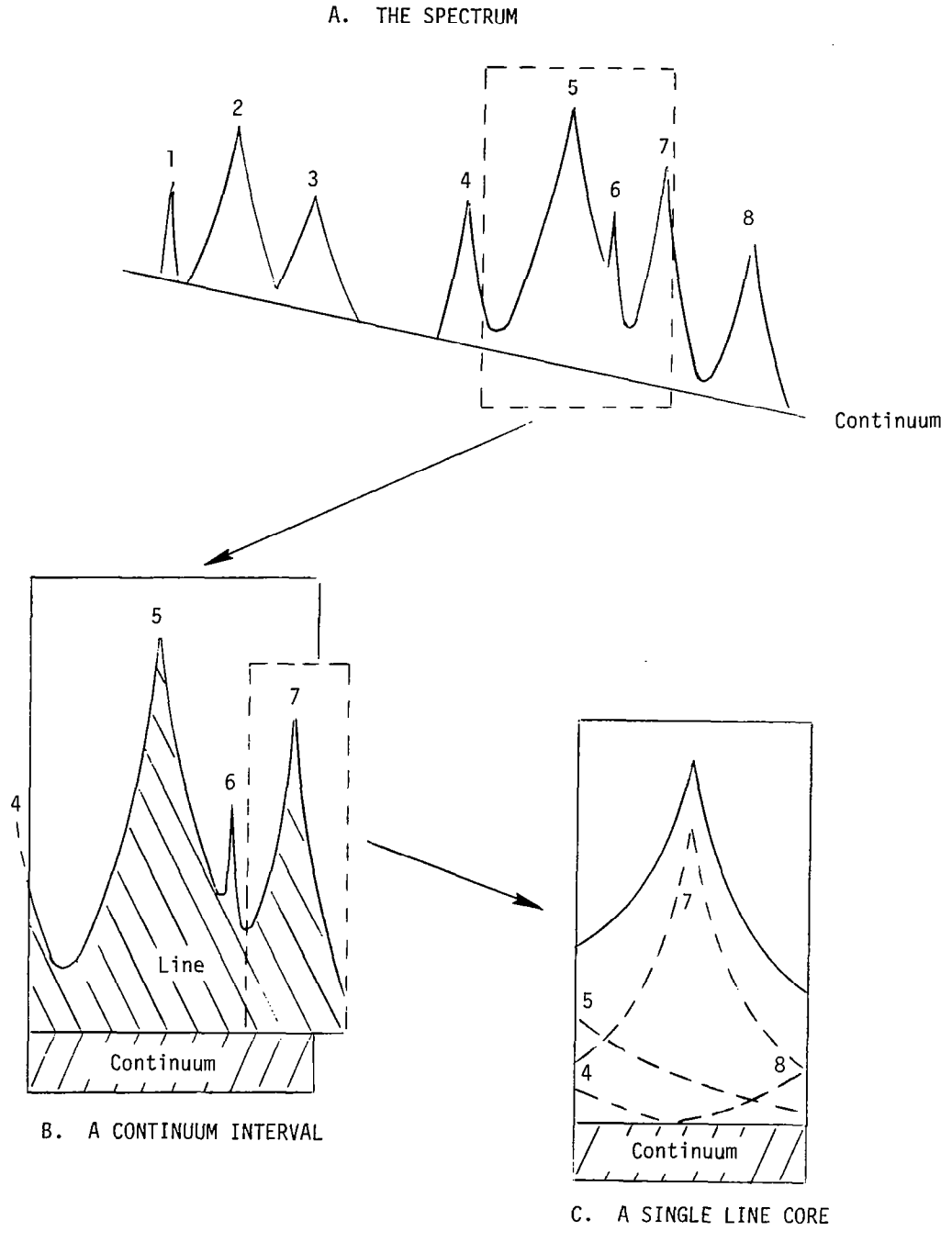


Figure 1. FREQUENCY-MARCHING METHOD

As mentioned previously, molecular lines are usually weak and heavily overlapped, and therefore are treated as pseudo-continuum, using either smeared band or bandless models. High line series in the atomic spectra are also treated as pseudo-continuum for the same reasons. High lines in the lower series, which represent transitions near the ionization threshold, are artificially included in the continuum by shifting the photoionization threshold.

In highly ionized plasmas, electron and ion impacts cause extreme line broadening, and most of the line transport is in the far wings. For lines of heavy atoms, suitable accuracy is obtained by using Lorentz line profiles with empirically curve-fit Stark half-widths; and for most hydrogen lines, with half-widths computed using the electron damping relation of Griem (15). However, emission from the strong hydrogen lines, notably the first two lines of the Lyman and Balmer series, can under certain plasma conditions dominate the radiative transport, and more detailed treatment is required.

Good experimental and theoretical data are available for the core regions of the strong hydrogen lines and have been tabulated by Griem (16) and Kepple and Griem (17). In the far wings, however, ion impacts distort the line profile, and there is as yet no consensus on the treatment of this region. Much work has centered on the lowest level transition, the Lyman alpha line; this work is summarized in Figure 2. The data is correlated by a function of the form

$$b = c(\Delta\lambda/F_0)^{-5/2} \; R(\Delta\lambda) \tag{22}$$

where $F_0 = 2.61eN^{2/3}$, the Holtsmark field strength; and $R(\Delta\lambda)$ correlates the influence of ion and electron perturbers at the wavelength separation $\Delta\lambda$.

The theories presented are the two region (ion impact and quasistatic) development of Griem (16); the Unified Classical Path treatment of Vidal, Cooper, and Smith (18); and the semiclassical stochastic approach of Frisch and Brissaud (19). The experimental data include the pulsed shock tube data of Elton and Griem (20) in the near wing; and in the far wing the wall-stabilized arc data of Boldt and Cooper (21) and Fussman (22).

The divergent curve represents a correlation suggested by Griem (15) for astrophysical work. It has been used by several investigators for planetary entry analysis (ref. 1,5,6) but yields severe overestimates of line heating.

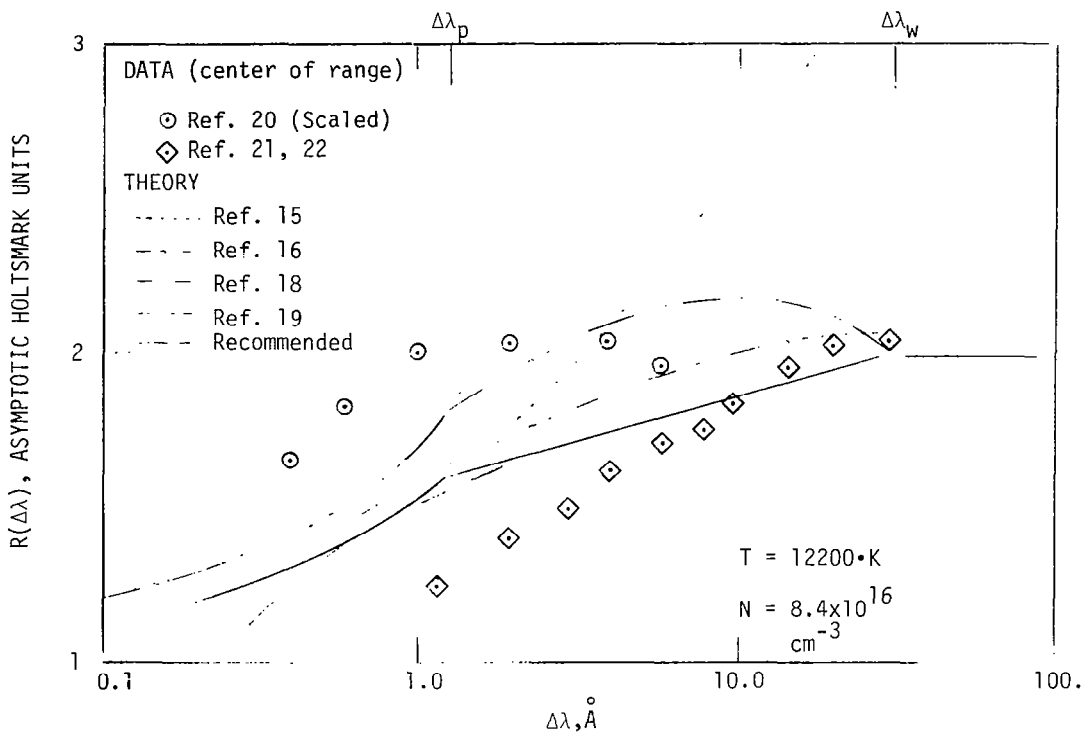


Figure 2. HYDROGEN LYMAN ALPHA LINE BROADENING

## 2.6 Hydrogen Line Transport Error Analysis

In view of the lack of consensus for the form of the far wings of the strong hydrogen lines and of their importance in outer planet entry calculations, it is prudent to assess the error that may arise from fortuitous choice of wing treatment. Consider the outer part of the flow field, from which most of the hydrogen radiation originates. This is closely approximated as a homogeneous layer with nonreflecting boundaries, and the unidirectional flux toward the wall at a point y in the layer may be found as follows.

$$\mu \approx b = c_1 \cdot R(\Delta\lambda) \cdot \Delta\lambda^{-5/2} \tag{23}$$

$$\tau \approx c_2 \cdot \mu \cdot y \tag{24}$$

substituting equations 9, 23, and 24 into 3, and assuming that the black-body emissive power $E_\nu$ is constant over the region of integration,

$$q_r^+ = 2E_\nu \int_0^\infty \{1 - \exp[c \cdot R(\Delta\lambda) \cdot \Delta\lambda^{-5/2}]\} d(\Delta\lambda) \tag{25}$$

If $R(\Delta\lambda)$ is constant, equation 25 may be integrated to yield

$$q_r^+ = 2E_\nu \cdot c^{0.4} \cdot R(\Delta\lambda)^{0.4} \cdot \Gamma(0.6) \tag{26}$$

Thus the dependence of the radiant energy on $R(\Delta\lambda)$ is less than square root. Because essentially all of the radiant transport takes place for $1 \leq R(\Delta\lambda) \leq 2$, the maximum error could be limited to 15% by setting $R(\Delta\lambda)$ to 1.6. However, the following expressions, adapted from Griem (15, 16), should limit the error to well under 10% for cases of interest:

$$R(\Delta\lambda) = [1 + R_{n,T}\, \Delta\lambda^{1/2}] \,, \quad \Delta\lambda \leq \Delta\lambda_p \tag{27a}$$

$$R(\Delta\lambda) = 2 \,, \quad \Delta\lambda \geq \Delta\lambda_w \tag{27b}$$

where the characteristic plasma frequency is,

$$\Delta\lambda_p = \lambda_c^{\,2} N^{1/2} \left(\frac{e^2}{\pi m c^2}\right)^{1/2} \tag{28}$$

and the quasistatic (impact cutoff) frequency is

$$\Delta\lambda_w = \lambda_c^2 \frac{kT}{hcn_u^2} \tag{29}$$

For the transition region, $\Delta\lambda_p < \Delta\lambda < \Delta\lambda_w$, Griem recommends logarithmic interpolation for $R(\Delta\lambda)$; linear interpolation is adequate for most problems, however.

## 2.7 CALICO Radiation Transport Program

The frequency-marching method presented above has been programmed in FORTRAN for the CDC 6000/CYBER 170 computer systems. The program, CALICO, is described in reference 23, and representative results are presented in the following sections. The method has proved to be almost as fast as the equivalent-width approach of reference 6, while retaining the detail of the finite difference method of the same source.

## Section 3

## RESULTS AND DISCUSSION

To test and characterize the frequency-marching method, a series of cases were run using the CALICO program for comparison with results from theory and from other investigators. In addition, the CALICO code was used in conjunction with the HYVIS program (24) to obtain wall heating results for a candidate heat shield material for a typical configuration. The cases are discussed below.

### 3.1 Isolated Line

The accuracy of the line flux integration is determined by the number and spacing of frequency grid points; by the width assigned to the line (as defined by equation 19); by the integration technique used; and by the method used to compute the layer emissivity. The effects of these parameters were investigated for an isolated line in a homogeneous layer with no continuum. The line was assigned the following nondimensional properties:

$$E_\nu = 1(eV)^{-1}$$

$$\gamma = \pi$$

$$S = \pi^2 \tau_c$$

The optical thickness of the layer at the frequency of the line center, $\tau_c$, was varied parametrically.

Results are presented in Figure 3 for a weak line, a strong line, and an "average" line. Emissivities calculated using the exponential approximation (equation 9) were compared to exact emissivities computed using a series expansion of the third-order exponential integral. "True" values for the integrated flux were obtained by using exact emissivities and sufficient frequency grid points to obtain convergence (typically, 11 to 12 on each side of the line center). Equivalent-width values were obtained using standard relations for weak and strong lines.

As expected, the exponential approximation overestimates the flux emanating from all but weak lines. It is also not too surprising that increasing the line width factor, $a_2$, requires increasing the number of grid points to avoid serious overprediction of the flux.

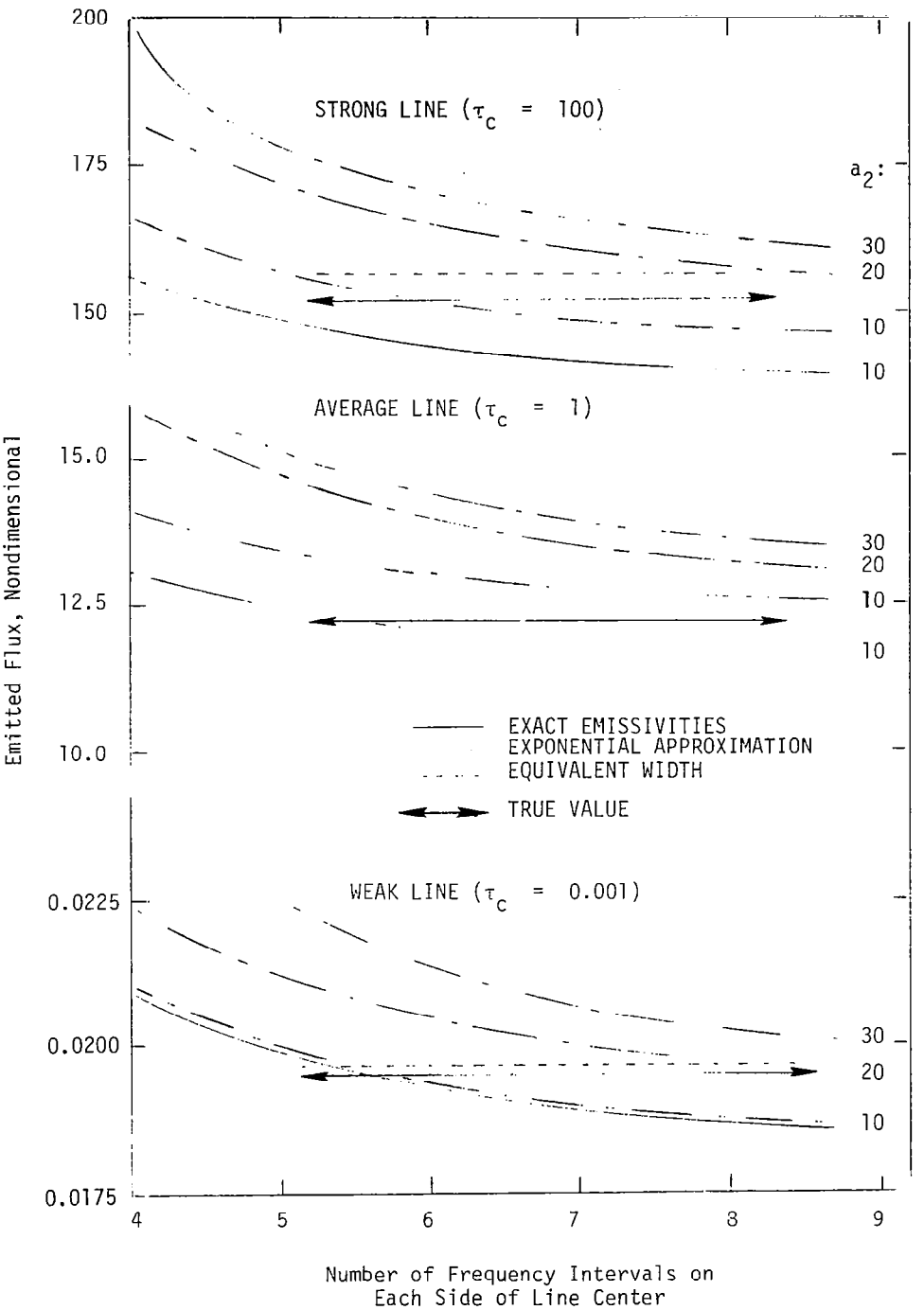


Figure 3. FLUX FROM AN ISOLATED LINE

Overall, the results indicate that the trapezoidal integration is quite satisfactory if the exponential approximation for emissivity is employed in conjunction with five to seven frequency intervals on each side of the line center.

### 3.2 Uniform Hydrogen-Helium Atmosphere

Perhaps the most detailed analyses of radiant heating in the hydrogen-helium atmospheres characteristic of the outer planets have been performed by Stickford (reference 1), and this work is the basis of the multiband engineering model of Poon (2). Poon's results for uniform slabs of simple composition are useful for checking the transport mechanism code of detailed models.

The case chosen for comparison has the following properties.

| | |
|---|---|
| Composition | 85% H, 15% He by volume |
| Density | $0.103 \times 10^{-6}$ gm/cm$^3$ |
| Gas temperature | 15,000° K |
| Shock thickness | 1 cm to 30 cm (parametric) |
| Cold wall | |

Photoionization and free-free continuum radiation are considered, along with 30 or so of the strongest lines.

Results obtained using the CALICO code are compared with Poon's in Figure 4. Agreement is excellent for the thicker layers; for the thin layers, however, the present method predicts considerably higher continuum fluxes. This difference was traced to the hydrogen photoionization treatment. Because the ground state threshold frequency is too high to influence wall heating in realistic problems, it is treated approximately by CALICO. Use of accurate Gaunt factors produced good agreement between the two methods.

Poon's multiband model requires approximately 1800 computations for this problem, whereas the present detailed method requires 3300 (1 to 2 seconds computing time on the CDC CYBER 175). The multiband model requires careful selection (by hand) of the band borders to avoid errors in the line flux computation; CALICO automates this procedure. Use of the present approach, considering only the strongest lines, offers an attractive alternative to multiband engineering models.

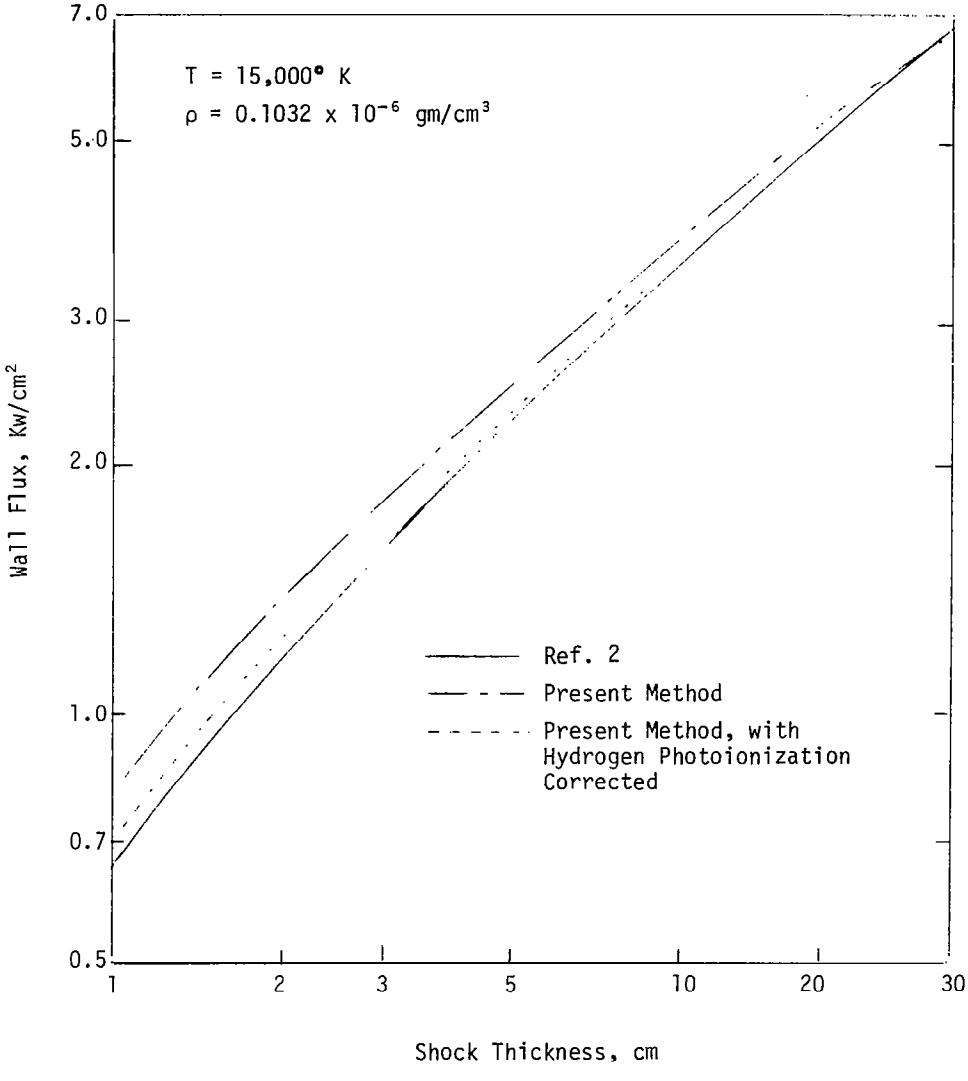


Figure 4. A UNIFORM HYDROGEN-HELIUM SLAB

### 3.3 Temperature-Varying $CO_2$ - $N_2$ Atmosphere

To obtain a comparison with the RAD/69 code of Nicolet, results were obtained for Case 2 of reference 14, using the present method. This case, described in Table 1, may be regarded as representative of the inviscid flow region about a Venus entry probe. Wall heating results are presented in Table 2. These show about only a 2% difference between CALICO and RAD/69 for continuum heating, but more than 10% for line heating. Since the continuum models are identical, the small disagreement in continuum fluxes may be attributed to differences in the chemistry models. Much of the line flux difference is caused by RAD/69 seriously over-predicting the flux of multiple (property-averaged high series) lines if they are overlapped. Introducing the RAD/69 approximation into the CALICO model reduces the difference in line flux to less than 5%, which can be attributed to differences in the chemistry models (2%), line property data, and integration procedure.

Case 1 of reference 13, also a $CO_2$ -$N_2$ atmosphere, was run to obtain timing comparisons with Nicolet's RAD/73 code. Because of several errors in line group boundary placement in the case presented in reference 13, the flux results could not be compared. The timings, however, can be compared and are presented in Table 3. These indicate that detailed radiation results can be obtained using the present method for about the same computational effort as the RAD/73 equivalent-width method.

While running these cases, it was noted that increasing the line width factor, $a_2$, in equation 19, caused the total line flux to increase almost without limit. Investigation showed that this was caused by the strong, narrow, low-level carbon lines. The frequency grid for these cases was chosen for the hottest part of the layer, where the lines were broadest. This causes overprediction of the flux near the wall, which is aggravated by increasing the line-width factor. It is recommended that values of the line-width factor greater than 10 be avoided.

### 3.4 Jovian Entry with Massive Blowing

To calculate the stagnation point wall heating and radiation blockage by ablation products for a Jovian orbital probe with a carbon-phenolic shield, the CALICO program was coupled to the HYVIS viscous shock layer program. Twenty spatial stations, 50 continuum frequency nodes, and 126 atomic lines (including 15 hydrogen) were used in the radiation calculation; this required 9 seconds computation time per iteration on the CDC CYBER 175. Entry conditions and essential line heating results are presented in Figure 5.

Table 1

$CO_2$ - $N_2$ ATMOSPHERE - FLOW FIELD DESCRIPTION

| Station | Position (cm) | Temperature $^oK$ | Pressure (atm)* | Elemental Mass Fractions | | |
|---|---|---|---|---|---|---|
| | | | | C | O | N |
| 1 | 0 | 5,000 | 1.0 | 0.068 | 0.182 | 0.750 |
| 2 | 0.047 | 6,000 | 1.0 | 0.068 | 0.182 | 0.750 |
| 3 | 0.118 | 7,000 | 1.0 | 0.068 | 0.182 | 0.750 |
| 4 | 0.237 | 8,000 | 1.0 | 0.068 | 0.182 | 0.750 |
| 5 | 0.474 | 9,000 | 1.0 | 0.068 | 0.182 | 0.750 |
| 6 | 0.948 | 10,000 | 1.0 | 0.068 | 0.182 | 0.750 |
| 7 | 2.11 | 10,500 | 1.0 | 0.068 | 0.182 | 0.750 |
| 8 | 4.74 | 11,000 | 1.0 | 0.068 | 0.182 | 0.750 |
| 9 | 7.37 | 11,500 | 1.0 | 0.068 | 0.182 | 0.750 |
| 10 | 10.0 | 12,000 | 1.0 | 0.068 | 0.182 | 0.750 |

*1 atm = $1.013 \times 10^5$ Pa.

Table 2

$CO_2$ - $N_2$ ATMOSPHERE - WALL RADIATIVE HEATING

| Method | Continuum ($w/cm^2$) | Line ($w/cm^2$) | Total |
|---|---|---|---|
| RAD/69 | 1324 | 853 | 2177 |
| CALICO | 1304 | 761 | 2065 |
| MODIFIED CALICO | 1304 | 815 | 2119 |

Table 3

$CO_2$ - $N_2$ ATMOSPHERE - CASE TIMINGS

| Method | RAD/73 | | CALICO |
|---|---|---|---|
| | Finite Difference | Equivalent Width | Finite Difference |
| Computer | UNIVAC 1108 | | CDC 6600 |
| CPU time | 86.1 | 10.7 | 9.8 |

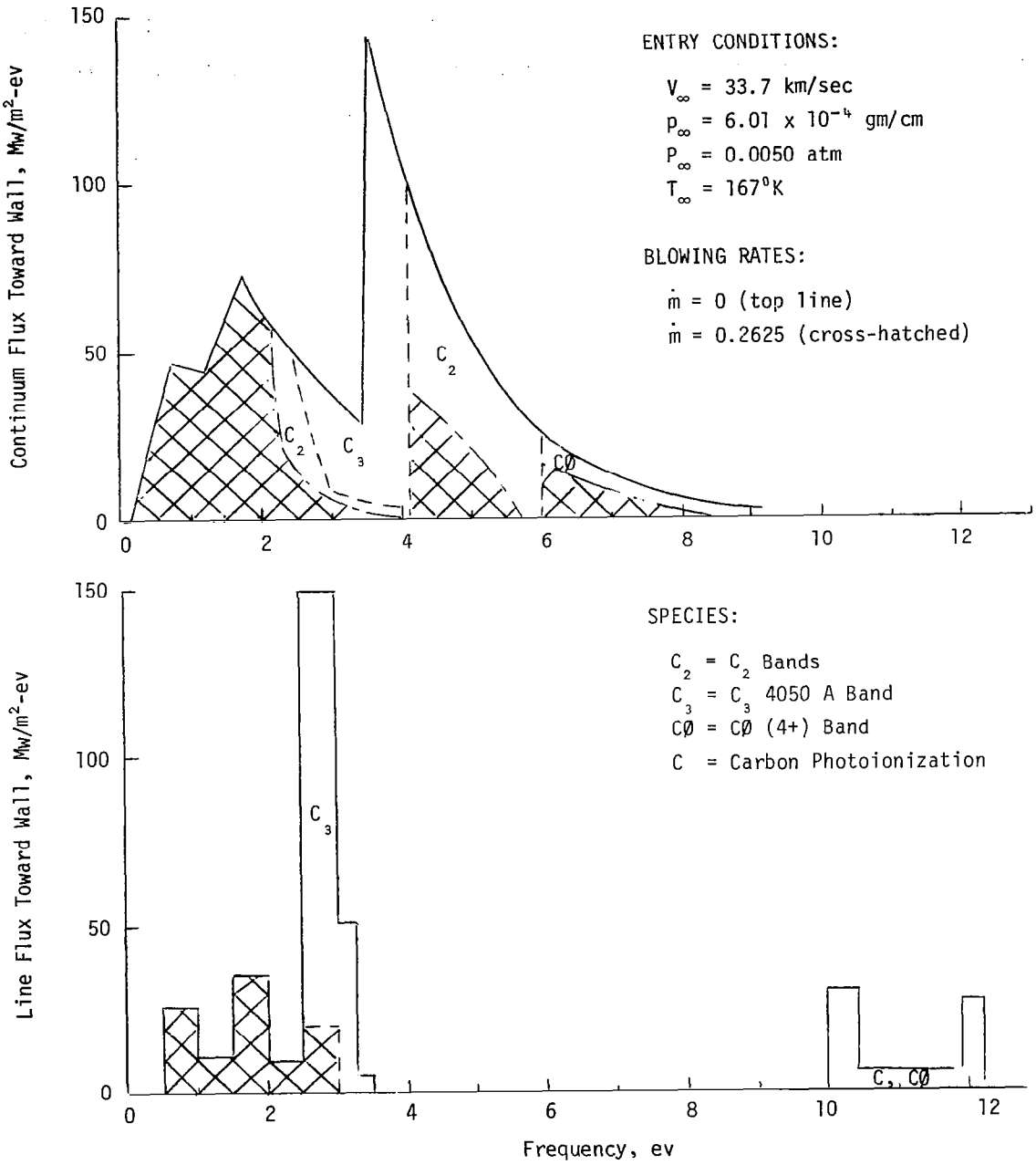


Figure 5. Stagnation Point Radiation Blockage by Carbon Species for Jovian Entry

## Section 4

## CONCLUSIONS

A frequency marching method has been presented for calculating nongrey radiative fluxes in plane-parallel slabs accurately and economically, while avoiding several approximations and limiting assumptions of existing models. The method allows detailed consideration for benchmark purposes of all the radiation mechanisms of importance in low-temperature plasmas, but may be easily detuned for engineering calculations. Results have been presented to characterize the method and build confidence in it. An example of the coupling of the method with a flow field program has been discussed.

The power and ease of application of the present method should facilitate substantial improvements in planetary entry vehicle analysis and design capability.

## Section 5

## REFERENCES


1. Stickford, G. H., and Menard, W. A., "Bow Shock Composition and Radiation Intensity Calculations for a Ballistic Entry into the Jovian Atmosphere," AIAA Paper No. 68-787, AIAA Third Thermophysics Conference, Los Angeles, California, June 1968.

2. Poon, P. T. Y., "Energy Transfer by Radiation in Non-gray Atomic Gases in Isothermal and Non-isothermal Slabs," AIAA Paper No. 75-702, AIAA Tenth Thermophysics Conference, Denver, Colorado, May 1975.

3. Page, W. A., "Aerodynamic Heating for Probe Vehicles Entering the Outer Planets," AAS Paper No. AAS-71-144, AAS 17th Annual Meeting, Seattle, Washington, June 1971.

4. Wilson, K. H., Woodward, H., Tauber, M., and Page, W. A., "Jupiter Probe Heating Rates," unpublished paper presented at the Symposium on Hypervelocity Radiating Flow Fields for Planetary Entry, Jet Propulsion Laboratory, Pasadena, California.

5. Nicolet, W. E., "Advanced Methods for Calculating Radiation Transport in Ablation-Product Contaminated Boundary Layers," CR-1656, NASA, 1970.

6. Nicolet, W. E., "Rapid Methods for Calculating Radiation Transport in the Entry Environment," CR-2525, NASA, 1975.

7. Nicolet, W. E., "Aerothermodynamic Environment for Jovian Entry Conditions," AIAA Paper No. 75-672, AIAA Tenth Thermophysics Conference, Denver, Colorado, May 1975.

8. Nicolet, W. E., Morse, H. L., and Vojvodich, N. S., "Outer Planet Probe Entry Thermal Protection: Part I: Aerothermodynamic Environment," AIAA Paper No. 74-700, AIAA/ASME 1974 Thermophysics and Heat Transfer Conference, Boston, Massachusetts, July 1974.

9. Sutton, K., "Radiative Heating About Outer Planet Entry Probes," AIAA Paper No. 75-183, AIAA Thirteenth Aerospace Sciences Meeting, Pasadena, California, January 1975.

10. Moss, J. N., Anderson, E. C., and Bolz, C. W., "Viscous-Shock-Layer Solutions With Radiation and Ablation Injection for Jovian Entry," AIAA Paper No. 75-671, AIAA Tenth Thermophysics Conference, Denver, Colorado, May 1975.

11. Olstad, W. E., "A Thick-Thin Approximation for Radiative Transfer," AIAA Paper No. 73-716, AIAA Eighth Thermophysics Conference, Palm Springs, California, July 1973.

12. Bolz, C. W., "An Algorithm for Selecting a Radiation Transport Subgrid for Ablation and Radiation Coupled Hypersonic Viscous-Shock-Layer Problems," CR-144957, NASA, 1976.

13. Nicolet, W. E., "User's Manual for RAD/EQUIL/1973, A General Purpose Radiation Transport Program," CR-132470, NASA, 1973.

14. Nicolet, W. E., "User's Manual for the Generalized Radiation Transfer Code (RAD/EQUIL)," CR-116353, 1969, NASA.

15. Griem, H. R., "Stark Broadening of Higher Hydrogen and Hydrogenlike Lines by Electrons and Ions," Astrophysical J., Vol. 132, pp 883-893, 1960.

16. Griem, H. R., Plasma Spectroscopy, McGraw-Hill Book Co., New York, 1964.

17. Kepple, P., and Griem, H. R., "Improved Stark Profile Calculations for the Hydrogen Lines H-alpha, H-beta, H-gamma, and H-delta," Phys. Rev., Vol. 173, pp. 317-325, 1968.

18. Vidal, C. R., Cooper, J., and Smith, E. W., "Hydrogen Stark Broadening Calculations with the Unified Classical Path Theory," JQSRT, Vol. 10, pp. 1011ff., 1970.

19. Brissaud, A., and Frisch, U., "Theory of Stark Broadening - II, Exact Line Profile with Model Microfield," JQSRT, Vol. 11, pp. 1767-1783, 1971.

20. Elton, R. C., and Griem, H. R., "Measurement of Stark Profiles of the Lyman-alpha and Lyman-beta lines of Hydrogen in an Electromagnetic Shock Tube," Phys. Rev., Vol. 135, pp. A1550-A1559, 1964.

21. Boldt, Von G., and Cooper, W. S., "Messung des Linienflugelprofiles der Wasserstofflinie Lyman Alpha," Z. Naturforschung, Vol. 192, No. 7/8, pp. 968-978, July/August 1964.

22. Fussmann, G., "Measurement of the Line Profile of Lyman Alpha," Physics Letters, Vol. 41A, No. 2, pp. 155-156, September 1972.

23. Bolz, C. W., "User's Manual for the CALICO Program for Calculation of Line and Continuum Radiation in Low Temperature Plasma," CR-158910, NASA, 1979.

24. Bolz, C. W., "User's Guide and Programming Manual for the HYVIS Hypersonic Shock Layer Program," CR-158911, NASA, 1979.

| 1. Report No. | 2. Government Accession No. | 3. Recipient's Catalog No. |
|---|---|---|
| NASA CR-3046 | | |

| 4. Title and Subtitle | 5. Report Date |
|---|---|
| A Marching Method for Calculating Line and Continuum Radiation in High Energy Flow Fields | June 1979 |
| | 6. Performing Organization Code |

| 7. Author(s) | 8. Performing Organization Report No. |
|---|---|
| Charles W. Bolz, Jr. | |
| | 10. Work Unit No. |

| 9. Performing Organization Name and Address | 11. Contract or Grant No. |
|---|---|
| Computer Sciences Corporation<br>Hampton, VA 23665 | NAS1-12527 |
| | 13. Type of Report and Period Covered |
| 12. Sponsoring Agency Name and Address | Contractor Report |
| National Aeronautics and Space Administration<br>Washington, DC 20546 | 14. Sponsoring Agency Code |

15. Supplementary Notes

Langley Technical Monitor: James N. Moss

Topical Report

16. Abstract

A method is presented for calculating nongrey radiative fluxes and intensities in a highly ionized, low-temperature plasma with extreme line broadening. The method was developed to study radiative heating phenomena in the mass-injected hypersonic shock-layer environments characteristic of outer planet atmospheric entry, although it is not limited to such studies. The radiative properties model assumes local thermodynamic equilibrium and uses standard continuum and molecular band models. The atomic line model, however, uses a frequency-marching method for the frequency integration, which not only accounts completely for line overlapping (reabsorption) effects, but compares favorably in economy with the best equivalent-width methods. An assessment of hydrogen line-far-wing treatments, with recommendations for engineering models, is also presented.

| 17. Key Words (Suggested by Author(s)) | 18. Distribution Statement |
|---|---|
| Radiation<br>Continuum and line | Unclassified - Unlimited<br><br>Subject Category 34 |

| 19. Security Classif. (of this report) | 20. Security Classif. (of this page) | 21. No. of Pages | 22. Price* |
|---|---|---|---|
| Unclassified | Unclassified | 26 | $4.50 |

* For sale by the National Technical Information Service, Springfield, Virginia 22161

NASA-Langley, 1979